LETTER

Origin of *f*-orbital-bonding insensitivity to spin-orbit coupling in UO_2

To cite this article: Bo Gyu Jang *et al* 2015 *EPL* **112** 17012

A Letters Journal Exploring the Frontiers of Physics

October 2015

EPL, **112** (2015) 17012 www.epljournal.org
doi: 10.1209/0295-5075/112/17012

Origin of f-orbital-bonding insensitivity to spin-orbit coupling in UO_2

Bo Gyu Jang[1], Seung Ill Hyun[1], Moo Hwan Kim[2], Massoud Kaviany[2,3] and Ji Hoon Shim[1,2,4(a)]

[1] *Department of Chemistry, Pohang University of Science and Technology - Pohang 790-784, Korea*
[2] *Division of Advanced Nuclear Engineering, Pohang University of Science and Technology - Pohang 790-784, Korea*
[3] *Department of Mechanical Engineering, University of Michigan - Ann Arbor, MI 48109, USA*
[4] *Department of Physics, Pohang University of Science and Technology - Pohang 790-784, Korea*

received 17 August 2015; accepted in final form 4 October 2015
published online 23 October 2015

PACS 71.27.+a – Strongly correlated electron systems; heavy fermions
PACS 71.70.Ej – Spin-orbit coupling, Zeeman and Stark splitting, Jahn-Teller effect
PACS 71.20.-b – Electron density of states and band structure of crystalline solids

Abstract – The origin of negligible spin-orbit coupling effects on the ground-state properties of UO_2 is examined using the LDA+DMFT and the LSDA+U methods. Although the previous theoretical results neglecting the spin-orbit coupling (SOC) are in reasonable agreement with experiments, this insensitivity has not been investigated. Via the charge density distribution, we show that the SOC does not affect the U-O bonding states which are directly related to the bonding properties (*e.g.*, lattice constant, bulk modulus, and oxidation/reduction energies).

Introduction. – Uranium oxides play important roles in the nuclear industry. For efficient energy generation from nuclear fuel and long-term storage of their high-level radioactive wastes, the physical, chemical, and thermal properties of the uranium oxides, in particular uranium dioxide (UO_2), have been examined and evaluated extensively. Stoichiometric UO_2 has the fluorite (CaF_2) structure over a wide range of temperature (up to its melting temperature of $\sim 3125\,\mathrm{K}$) and pressure ($\sim 40\,\mathrm{GPa}$) [1,2]. UO_2 is a Mott-Hubbard insulator [3] due to its strong correlation among uranium $5f$-electrons, and shows an antiferromagnetic ordering of uranium ions below 30 K [4,5]. The theoretical studies of these compounds complement the experiments on these radioactive materials which require extensive time and resources. The density functional theory (DFT) approaches have been extensively performed on uranium compounds. However, the conventional DFT-based studies have failed to predict the correct physical and chemical properties of UO_2 because of the correlation effects in uranium $5f$-electrons. For example, they predict metallic behavior for UO_2 in contrast to the insulating behavior observed in experiments [6,7]. Recent theoretical studies use the LSDA method combined with the Coulomb interaction U (LSDA+U) as well as the hybrid DFT method. All these methods are developed in order to describe the correlation effects of uranium $5f$-electrons accurately. These yield relevant results for the structural, electronic, and magnetic properties in good agreement with the experimental results [8–12]. The more advanced techniques such as the dynamical mean-field theory (DMFT) and the self-interaction correction approaches are developed for the description of the many-body electronic structures of actinide compounds [13–15]. Among them, the LSDA+U is the most widely used method, because it can be easily implemented into the conventional DFT packages. The LSDA+U method is also widely applied to many correlated electron systems such as the transition metal oxides and rare-earth compounds [2,8,16–23].

There have been many theoretical studies of the uranium oxides with the LSDA+U method; however the effect of the SOC has not been clearly identified. Usually the SOC is ignored in predicting the physiochemical properties [2,20,24,25], because it is believed to have limited influence on the thermodynamic and structural properties [24]. However, the SOC is expected to be important for the description of the magnetic and electronic ground state, because the heavy elements have strong SOC contribution to the electronic structure. Indeed, the SOC effect has been reported to be important in structural properties such as the unusual simple cubic structure of α-polonium [26] and the thermal properties such as the

(a) E-mail: jhshim@postech.ac.kr

specific heat of bismuth [27]. So, there is a need to understand not only the strong correlation effects but also the contributions of the SOC to the physiochemical properties of the uranium oxides.

Here, we first verify the accuracy of the LSDA+U method by comparing its predictions with the LDA+DMFT method, then we compare the LSDA+U calculations with and without the SOC to examine its contribution to the predicted physiochemical properties. Finally, we discuss the origin of insensitivity to the SOC. We use the charge density distributions obtained with and without the SOC and examine the charge density along the U-O bonding, which is directly related to the mechanical and thermal properties of materials.

Methods. – *LDA+DMFT.* The LDA+DMFT method is a combination of the DFT and DMFT methods [28]. The detail of the DMFT implementation to the DFT method has been introduced in ref. [29]. The effective one-particle Hamiltonian is generated by the LDA calculation and the Coulomb interaction among the correlated orbitals is taken into account by the DMFT calculations. The spectral function is obtained from the electron Green's function $A(\mathbf{k},\omega) = (G^{\dagger}(\mathbf{k},\omega) - G(\mathbf{k},\omega))/(2\pi i)$, where

$$G(\mathbf{k},\omega) = \frac{1}{O_{\mathbf{k}}(\omega+\mu) - H_{\mathbf{k}} - \Sigma(\omega)}. \qquad (1)$$

Here, the one-particle Hamiltonian $H_{\mathbf{k}}$ and overlap matrix $O_{\mathbf{k}}$ is obtained from the LDA method. The electron correlation effect is treated by the self-energy $\Sigma(\omega)$, which is computed by using the NCA (non-crossing approximation) impurity solver. We use the on-site Coulomb interaction $U = 4.0\,\mathrm{eV}$ on the U $5f$-electrons and the Hund coupling constant $J = 0.56\,\mathrm{eV}$. The temperature is prescribed as 23 K.

LSDA+U. The LSDA+U method, where U designation addresses the correlation effect for uranium $5f$-electrons, is selected in the WIEN2k package [30] that used the full-potential augmented plane wave plus local orbital as the basis. Inclusion of the on-site Coulomb repulsion is represented by the Hubbard model consisting of a mean-field solution and a fluctuation term due to Coulomb interaction [21,31,32], *i.e.*

$$E_{LSDA+U} = E_{LSDA}[\{\varepsilon_i\}] + \frac{(U-J)}{2}\sum_{l,j,\sigma}\rho^{\sigma}_{lj}\rho^{\sigma}_{jl}, \qquad (2)$$

where $\{\varepsilon_i\}$ are the Kohn-Sham eigenvalues, ρ^{σ}_{lj} is the density matrix of d or f orbital, σ refers to the spin direction, and U and J are model parameters for the Coulomb and exchange interactions, respectively, which can be obtained from the first-principles calculations [33–35]. Here $(U-J)$ is the same as the effective U (U_{eff}). The value of U_{eff} has been optimized by adjusting the calculated band gap to the experimental value.

For all uranium compounds, the same U_{eff} value is used. The U_{eff} value is the property of localized uranium f orbital, so it does not change a lot depending on the compounds. Although there could be small variations in the optimal U_{eff} value depending on the compounds, this does not affect the tendency much.

Results and discussion. – *Crystal structures of uranium oxides.* Among the actinide oxides, AO_2, A_2O_3, and A_4O_9 (A = actinide elements) are generally the most important compounds. The UO_2 has a cubic fluorite structure as the ground-state structure with space group $Fm\bar{3}m$ which is used here. The large octahedral holes are a typical feature of the fluorite structure, and they are easily occupied by defects (*e.g.*, interstitial ions) [24]. The $Fm\bar{3}m$ can transform to an orthorhombic structure (*Pnma*) under high pressure (beyond 40 GPa) [1,23,36].

Although UO_2 shows the Jahn-Teller distortion with the $3\mathbf{k}$ antiferromagnetic (AFM) order below the Néel temperature, we use the undistorted fluorite structure with the $1\mathbf{k}$ AFM ordering as done in many previous theoretical studies, which is good enough for the discussion of the role of the SOC in UO_2 due to very small energy difference [37].

U_4O_9 has three phases known as α, β, and γ between room temperature and 1273 K. However, its structure is rather complicated, a fluorite-type $4\times4\times4$ supercell as the unit cell [38,39], a challenge for the direct *ab initio* calculations (it requires extensive computation).

Therefore, Petit *et al.* simplified the unit cell by adding an O atom in the octahedral cavity creating the isotope compound U_4O_9 [15], *i.e.*, a defective UO_2 [22], which is also used here. The calculated lattice constant is 5.38 Å which is slightly smaller than the experimental value (5.44 Å) and may be due to the simplified U_4O_9 structure and this is also found by others [20,23].

The bulk U_2O_3 and Np_2O_3 do not exist naturally. However, beyond Pu, the actinide sesquioxides exist and have three different structures, *i.e.*, the A, B, and C types. For testing the reduction energy, the crystal structure of Pu_2O_3 is used to construct that of U_2O_3 [15–18]. The Pu_2O_3 is synthesized only in two form, α-Pu_2O_3 (C type) and β-Pu_2O_3 (A type) [15]. So, the crystal structures of α-U_2O_3 (C type) and β-U_2O_3 (A type) are constructed by using the lattice and internal parameters of Pu_2O_3. After optimization of the lattice constants and internal parameters, several properties of the U_2O_3 are calculated.

Although there is no experimental result for U_4O_9 and U_2O_3, the predicted bulk moduli show the same trend as those of Geng *et al.* [22]. They reported that although there is a structure dependence, with increase in the oxidation up to U_4O_9, the bulk modulus increases.

Electronic structure. First we compare the LDA+DMFT result and the LSDA+U result to confirm that the LSDA+U method correctly describes the correlation effects of the uranium $5f$-electrons. The results are shown in fig. 1(a). Our LDA+DMFT result agrees well with a previous calculation [40]. The LSDA+U results also well describe the correlation effect of the U $5f$-electrons. Especially, the lower Hubbard band originated from the

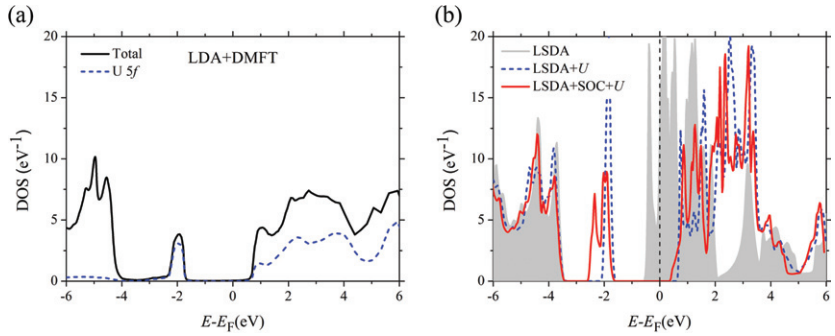

Fig. 1: (Color online) (a) Predicted electronic density of states for UO_2 from LDA+DMFT ($U = 4\,\text{eV}$, $J = 0.56\,\text{eV}$, 23 K). The black solid line and the blue dotted line represent the total DOS and the partial DOS of U $5f$ orbitals, respectively. (b) Predicted electronic density of states for UO_2 from LSDA (grey filled line), LSDA+U (blue dotted line), and LSDA+SOC+U (red solid line). For clarity, the Fermi level is indicated with black dashed line.

Table 1: Calculated properties of UO_2 and comparison with available experimental and predicted results.

	Experiments [1,43–46]	S.L. Dudarev [8,19] (LSDA+U, $U_{eff} = 4.0\,\text{eV}$)	Yun *et al.* [12] (GGA+U, $U_{eff} = 4.0\,\text{eV}$)	This work (LSDA+U, $U_{eff} = 4.5\,\text{eV}$)
Lattice constant a (Å)	5.46	5.37	5.44	5.45
Bulk modulus B (GPa)	207	202	209	212
Band gap energy (eV)	2.0	2.1	1.8	2.0
Magnetic moment (μ_B)	1.74	2.1	1.8	1.8

localized U $5f$-electrons is quantitatively described by the LSDA+U method as well in fig. 3. Also the small contribution of the U $5f$ orbital in the O p-band position, which cannot be ignored in the U-O bonding, is well captured by the LSDA+U method. We conclude that the LSDA+U method is appropriate for describing the physical and chemical properties of the UO_2. Later, we will discuss several properties predicted by the LSDA+U method.

The ground-state lattice constants of UO_2, obtained from the lattice relaxation, agree well with the experimental values and previous calculations. The calculated results are compared with the experimental [1,41–46] and calculated results [8,12,19,20,23], with good agreement as shown in table 1.

The change in the electronic structures with the inclusion of the SOC is shown in fig. 1(b), *e.g.*, the band gap energy with and without the SOC. Since the calculation without the SOC gives larger band gap than the one with SOC at the same U_{eff} value as shown in fig. 1(b), we use a larger U_{eff} (4.5 eV) compared to the previous studies ($U_{eff} = 4.0\,\text{eV}$) which did not consider the SOC [8,12,19,20,23,26,47] to reproduce the experimental band gap. Also the electronic DOS near the band gap is affected by the inclusion of the SOC, indicating the change in the transport properties depending on the doping (Fermi level). So, we expect that the excited-state properties to be affected by the inclusion of the SOC.

Ground-state properties. We investigate the SOC effect on the ground-state magnetic ordering by using the total energy calculation. In the PuO_2, it is reported that LSDA+U method without the SOC fails to capture the paramagnetic ground state of PuO_2 [48]. The ground-state lattice constant and the bulk modulus are determined by fitting the calculated total energies with the Birch-Murnaghan equation of state.

Non-magnetic (NM), ferromagnetic (FM), and antiferromagnetic (AFM) configuration are considered. For reference, in the AFM case, the spin magnetic moments are 1.79 μ_B and 1.83 μ_B with and without the SOC, and the orbital magnetic moments are 3.37 μ_B and 0, respectively.

Figures 2(a) and (b) show the calculated energy as a function of lattice constant, for the UO_2 with and without the SOC. The energies are referenced to the fitted ground-state energies for the AFM configuration. Unlike the PuO_2 case, the AFM configuration is correctly captured as the ground state for both cases. The ground-state energy of the NM configuration is much higher than that of magnetic configuration. (0.754 and 1.410 eV/U-atom for with and without SOC, respectively.)

The energy difference between the AFM and FM ordering is 3 and 10 meV/U-atom, with and without the SOC, respectively. These values are consistent with the Néel temperature of 30 K, assuming the mean-field approach of the Heisenberg model on an fcc lattice [49].

Table 2: Effect of the SOC on calculated lattice constant and bulk modulus of uranium oxides and comparison with available experimental results.

Compound	Lattice constant a (Å)			Bulk modulus B (GPa)		
	with SOC	w/o SOC	Exp.	with SOC	w/o SOC	Exp.
UO_2	5.45	5.44	5.46	212	235	207
U_4O_9	5.38	5.36	5.44	253	257	–
α-U_2O_3	7.66	7.61	–	166	172	–
β-U_2O_3	3.83	3.81	–	142	147	–

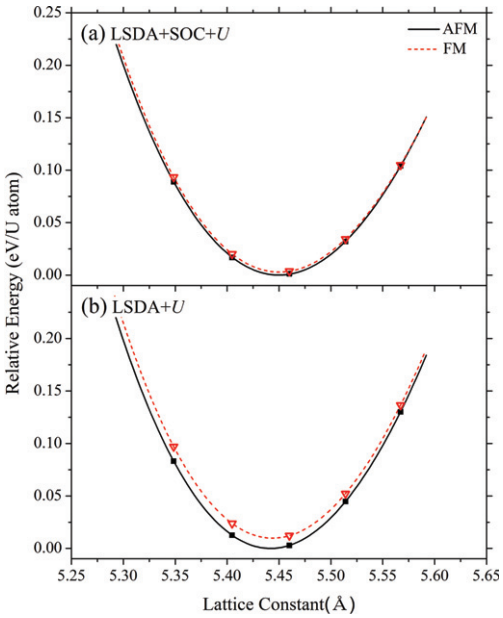

Fig. 2: (Color online) Total energy of UO_2 for AFM and FM magnetic ordering as a function of the lattice constant, using (a) LSDA+SOC+U, and (b) LSDA+U calculations.

The lattice constant and bulk modulus of other uranium oxides compounds are also calculated with and without the SOC and listed in table 2. Without the SOC the lattice constants are underestimated and the bulk moduli are overestimated, but the differences are not large. So, the calculations without the SOC give results in agreement with the experimental results (similar to previous studies not considering the SOC effect [8,12,19,20,23]).

The knowledge of the oxidation and reduction of UO_2 is important for a safe disposal of the nuclear wastes and possible chemical changes in the fuel material during the reactor operation. We verify these oxidation and reduction trends using the calculated total energies and examine the SOC effect on the oxidation and reduction energies. We assume 0 K to remove the entropy contribution in the free energy, so the oxidation/reduction energies are

$$E^{ox} = \frac{1}{4}E(U_4O_9) - E(UO_2) - \frac{1}{8}E(O_2), \quad (3)$$

$$E^{red} = \frac{1}{2}E(U_2O_3) + \frac{1}{4}E(O_2) - E(UO_2), \quad (4)$$

where E(A) is the total energy of compound A.

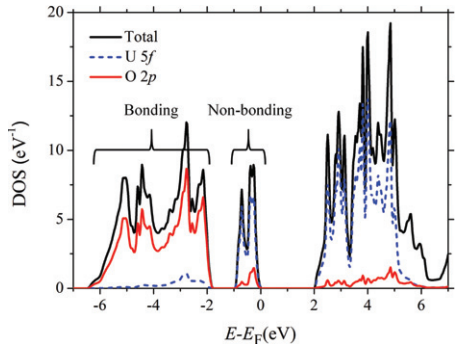

Fig. 3: (Color online) Density of states for UO_2. Black solid line, blue dotted line, and red solid line represent the total DOS, the partial DOS of U $5f$ orbitals, and the partial DOS of O $2p$ orbitals, respectively.

The calculated oxidation energy with the SOC is −1.36 eV/U-atom. This is reasonable considering UO_{2+x} is oxidized up to $x = 0.25$, U_4O_9, and its experimental oxidation energy −1.8 eV/U-atom [50]. The difference of about 0.46 eV is from the simplified U_4O_9 structure used, so the agreement is fair. The calculated oxidation energy without the SOC is −1.56 eV/U-atom which is slightly larger than the value calculated with the SOC. A previous study not including the SOC with the same structure, finds −1.4 (LSDA + U, U_{eff} = 4.0 eV) [23], −1.5 (GGA + U, U_{eff} = 4.0 eV) [9], and −1.9 eV/U-atom (LSDA + U, U_{eff} = 3.99 eV) [20]. All these are in a reasonable range compared to the experimental value.

The reduction energies with the SOC are 6.11 and 6.26 eV/U-atom when UO_2 is reduced to α-U_2O_3 and β-U_2O_3, respectively. The larger, positive reduction energies mean the U_2O_3 phase is very unstable compared to UO_2, when exposed to oxygen, reasonable since the U_2O_3 does not naturally exist.

The reduction energies without the SOC are 5.91 and 6.29 eV/U-atom, for α-U_2O_3 and β-U_2O_3. So, the reduction energies for UO_2 are not sensitive to the inclusion of the SOC effect. The Pu_2O_3 is obtained by partial reduction of PuO_2 at high temperatures [51]. The reduction energies are 1.72 (calculated with LSDA+U) [18] and 2.16 eV/U-atom (experiment) [52] when PuO_2 was reduced to α-Pu_2O_3 and β-Pu_2O_3. For the oxidation and reduction energies of UO_2, the calculations with and without the SOC result in a small difference.

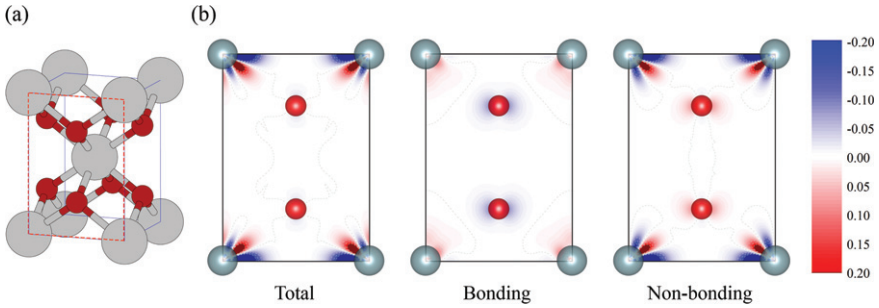

Fig. 4: (Color online) The calculated charge density distribution differences between the calculations with and without the SOC ($\rho_{\text{with SOC}} - \rho_{\text{w/o SOC}}$) for i) total, ii) prescribed bonding, and iii) non-bonding energy range. (a) The red dotted line indicates the (1 0 0) plane in the UO_2 unit cell. Gray and red spheres indicate the U and O atoms, respectively. (b) The charge density distribution in the (1 0 0) plane. Red and blue indicate positive and negative values and a darker color indicates larger differences. The unit is the number of electrons per unit volume ($Å^3$).

Insensitive SOC effects on charge density distribution. As mentioned above, the SOC is important in describing the electronic and magnetic properties of a heavy atom system, but the effect on the physiochemical properties of UO_2 are not as important. So we investigate the change of the bond charge density by including the SOC.

To verify the SOC effect on bonding and non-bonding states carefully, the partial charge densities are calculated for a prescribed bonding, the non-bonding energy range, and the total energy range. We assign the bonding (about $-6 \div -2$ eV) and non-bonding (about -1–0 eV) states in the valence bands of the UO_2, based on the previous XPS studies, as shown in fig. 3 [42,53]. The assigned non-bonding state, which is right below the Fermi level, has mainly the U $5f$ orbital characters. Although the assigned bonding states has small U $5f$ orbital characters, the U $5f$ orbital plays an important role in the U-O bonding. To verify the importance of the U $5f$ orbitals in the bonding, we employed the open-core method which treats the U $5f$-electrons as core electrons to remove their contribution to the bonding. The open-core calculation underestimates the volume by around 5%, so we can conclude that the contribution of the U $5f$ orbitals in bonding is crucial for the description of lattice properties.

Figures 4(a) and (b) show the charge density distribution differences between the results with and without the SOC ($\rho_{\text{with SOC}} - \rho_{\text{w/o SOC}}$). To examine the SOC effect on the U-O bonding, we analyze the charge density distribution on the (1 0 0) plane of the UO_2 unit cell which contains the U-O bonding (fig. 4(a)). For the bonding energy range, there is a very small difference between the two results. Especially, there is a negligible difference in the middle of the U and O atoms, which is important for the U-O bonding properties. The charge density difference over the entire energy range is not negligible, however this difference mainly comes from the non-bonding energy range which is not significant for the bonding. So we can conclude that the charge density in the bonding energy range is not affected much by including the SOC, while the charge density in the non-bonding region is affected by the inclusion of the SOC. These results indicate that the non-bonding states, from the U $5f$ orbital character, are affected more by the SOC, while the U-O bonding states are not significantly changed by the SOC. The charge density distribution is directly related to the bond strength, which determines most of physiochemical properties such as lattice constant, bulk modulus, and redox energy. For comparison, the α-Po, whose bonding properties are strongly affected by the inclusion of the SOC, shows a significant difference in the charge density distribution by the SOC effect [54].

Conclusion. – We have verified the role of the SOC on the physiochemical properties of uranium oxides. We confirmed that the LSDA+U method results agree well with the results of the LDA+DMFT in the spectral function. So, we analyzed several physiochemical properties of the uranium oxides using the LSDA+U method. The excited-states properties, such as the electronic band gap, the DOS and the magnetic moment, are sensitive to the inclusion of the SOC. On the other hand, the physiochemical properties, including the lattice constant, the bulk modulus, and the oxidation/reduction energy, are not. We found that the SOC does not affect the charge density of the U-O bonding states, which in turn determines the thermophysical properties. So the SOC should be carefully excluded only for the analysis of the ground-state properties.

* * *

This research was supported by the Radiation Technology R&D Program through NRF (2013M2B2A9A03051257), the Global Frontier Program through the Global Frontier Hybrid Interface Materials (2013M3A6B1078870), and the Supercomputing Center/Korea Institute of Science and Technology Information with supercomputing resources including technical support (KSC-2012-C1-029)

REFERENCES

[1] Idiri M., Le Bihan T., Heathman S. and Rebizant J., *Phys. Rev. B*, **70** (2004) 014113.

[2] Geng H. Y., Chen Y., Kaneta Y. and Kinoshita M., *Phys. Rev. B*, **75** (2007) 054111.
[3] Kotani A. and Yamazaki T., *Prog. Theor. Phys. Suppl.*, **108** (1992) 117.
[4] Lynds L., *J. Inorg. Nucl. Chem.*, **24** (1962) 1007.
[5] Cracknell A. P. and Daniel M. R., *Proc. Phys. Soc.*, **92** (1967) 705.
[6] Kelly P. J. and Brooks M. S. S., *J. Chem. Soc. Faraday Trans. II*, **83** (1987) 1189.
[7] Petit T., Morel B., Lemaignan C., Pasturel A. and Bigot B., *Philos. Mag. B*, **73** (1996) 893.
[8] Dudarev S. L., Manh D. N. and Sutton A. P., *Philos. Mag. B*, **75** (1997) 613.
[9] Iwasawa M., Chen Y., Kaneta Y., Ohnuma T., Geng H.-Y. and Kinoshita M., *Mater. Trans.*, **47** (2006) 2651.
[10] Dorado B., Amadon B., Freyss M. and Bertolus M., *Phys. Rev. B*, **79** (2009) 235125.
[11] Kudin K. N., Scuseria G. E. and Martin R. L., *Phys. Rev. Lett.*, **89** (2002) 266402.
[12] Yun Y., Kim H., Kim H. and Park K., *Nucl. Eng. Technol.*, **37** (2005) 6.
[13] Shim J. H., Haule K. and Kotliar G., *Nature*, **446** (2007) 513.
[14] Savrasov S. Y., Kotliar G. and Abrahams E., *Nature*, **410** (2001) 793.
[15] Petit L., Svane A., Szotek Z., Temmerman W. M. and Stocks G. M., *Phys. Rev. B*, **81** (2010) 045108.
[16] Jomard G., Amadon B., Bottin F. and Torrent M., *Phys. Rev. B*, **78** (2008) 075125.
[17] Sun B., Zhang P. and Zhao X. G., *J. Chem. Phys.*, **128** (2008) 084705.
[18] Shi H. L. and Zhang P., *J. Nucl. Mater.*, **420** (2012) 159.
[19] Dudarev S. L., Botton G. A., Savrasov S. Y., Szotek Z., Temmerman W. M. and Sutton A. P., *Phys. Status Solidi*, **166** (1998) 429.
[20] Andersson D. A., Lezama J., Uberuaga B. P., Deo C. and Conradson S. D., *Phys. Rev. B*, **79** (2009) 024110.
[21] Liechtenstein A. I., Anisimov V. I. and Zaanen J., *Phys. Rev. B*, **52** (1995) 5467.
[22] Geng H. Y., Song H. X., Jin K., Xiang S. K. and Wu Q., *Phys. Rev. B*, **84** (2011) 174115.
[23] Geng H. Y., Chen Y., Kaneta Y., Iwasawa M., Ohnuma T. and Kinoshita M., *Phys. Rev. B*, **77** (2008) 104120.
[24] Pickard C. J., Winkler B., Chen R. K., Payne M. C., Lee M. H., Lin J. S., White J. A., Milman V. and Vanderbilt D., *Phys. Rev. Lett.*, **85** (2000) 5122.
[25] Freyss M., Petit T. and Crocombette J.-P., *J. Nucl. Mater.*, **347** (2005) 44.
[26] Kang C.-J., Kim K. and Min B. I., *Phys. Rev. B*, **86** (2012) 054115.
[27] Díaz-Sánchez L. E., Romero A. H., Cardona M., Kremer R. K. and Gonze X., *Phys. Rev. Lett.*, **99** (2007) 165504.
[28] Kotliar G., Savrasov S. Y., Oudovenko V. S., Parcollet O. and Marianetti C. A., *Rev. Mod. Phys.*, **78** (2006) 865.
[29] Haule K., Yee C. and Kim K., *Phys. Rev. B*, **81** (2010) 195107.
[30] Blaha P., Schwarz K., Madsen G., Kvasnicka D. and Luitz J., *WIEN2k, an Augmented Plane Wave + Local Orbitals Program for Calculating Crystal Properties* (Karlheinz Schwarz, Technische Universität Wien) 2001, ISBN 3-9501031-1-2.
[31] Anisimov V. I., Zaanen J. and Andersen O. K., *Phys. Rev. B*, **44** (1991) 943.
[32] Anisimov V. I., Solovyev I. V., Korotin M. A., Czyżyk M. T. and Sawatzky G. A., *Phys. Rev. B*, **48** (1993) 16929.
[33] Aryasetiawan F., Karlsson K., Jepsen O. and Schönberger U., *Phys. Rev. B*, **74** (2006) 125106.
[34] Miyake T., Aryasetiawan F. and Imada M., *Phys. Rev. B*, **80** (2009) 155134.
[35] Kutepov A., Haule K., Savrasov S. Y. and Kotliar G., *Phys. Rev. B*, **82** (2010) 045105.
[36] Yu J., Devanathan R. and Weber W. J., *J. Phys.: Condens. Matter*, **21** (2009) 435401.
[37] Dorado B., Jomard G., Freyss M. and Bertolus M., *Phys. Rev. B*, **82** (2010) 035114.
[38] Bevan D. J. D., Grey I. E. and Willis B. T. M., *J. Solid State Chem.*, **61** (1986) 7.
[39] Cooper R. I. and Willis B. T. M., *Acta Crystallogr. A*, **60** (2004) 322.
[40] Yin Q., Kutepov A., Haule K., Kotliar G., Savrasov S. Y. and Pickett W. E., *Phys. Rev. B*, **84** (2011) 195111.
[41] Baer Y. and Schoenes J., *Solid State Commun.*, **33** (1980) 885.
[42] Veal B. and Lam D., *Phys. Rev. B*, **10** (1974) 4902.
[43] Verbist J., Riga J., Pireaux J. J. and Caudano R., *J. Electron. Spectrosc. Relat. Phenom.*, **5** (1974) 193.
[44] Cox L. E., *J. Electron. Spectrosc. Relat. Phenom.*, **26** (1982) 167.
[45] Martin D. G., *High Temp. High Press.*, **21** (1989) 13.
[46] Benedict U., Andreetti G. D., Fournier J. M. and Waintal A., *J. Phys. Lett. (Paris)*, **43** (1982) 171.
[47] Kim H., Kim M. H. and Kaviany M., *J. Appl. Phys.*, **115** (2014) 123510.
[48] Nakamura H., Machida M. and Kato M., *Phys. Rev. B*, **82** (2010) 155131.
[49] McKenzie S., Domb C. and Hunter D. L., *J. Phys. A*, **15** (1982) 3899.
[50] Chevalier P. Y., Fischer E. and Cheynet B., *J. Nucl. Mater.*, **303** (2002) 1.
[51] *The Plutonium-Oxygen and Uranium-Plutonium-Oxygen Systems: A Thermochemical Assessment*, IAEA Technical Reports Series, No. 79 (International Atomic Energy Agency, Vienna) 1967.
[52] Haschke J. M., Allen T. H. and Morales L. A., *Los Alamos Sci.*, **26** (2000) 252.
[53] Teterin Y. A., Kulakov V. M., Baev A. S., Nevzorov N. B., Melnikov I. V., Streltsov V. A., Mashirov L. G., Suglobov D. N. and Zelenkov A. G., *Phys. Chem. Miner.*, **7** (1981) 151.
[54] Min B. I., Shim J. H., Park M. S., Kim K., Kwon S. K. and Youn S. J., *Phys. Rev. B*, **73** (2006) 132102.